

Evaluation of Reduced *n*-Heptane Mechanisms in Dual-Fuel Combustion

Jiun Cai Ong^{1*}, Jens Honore Walther^{1,2}, Xue-Song Bai³, Kar Mun Pang⁴

1 Department of Mechanical Engineering, Technical University of Denmark, Nils Koppels Allé, 2800 Kgs, Lyngby, Denmark.

2 Computational Science and Engineering Laboratory, ETH Zürich, Clausiusstrasse 33, Zürich CH-8092, Switzerland.

3 Department of Energy Sciences, Lund University, 22100 Lund, Sweden.

4 MAN Energy Solutions, Teglholmegade 41, 2450 København SV, Denmark.

*Corresponding author: jcong@mek.dtu.dk

ABSTRACT

Numerical simulations are carried out to evaluate the performance of different reduced *n*-heptane mechanisms in dual-fuel combustion. Three reduced *n*-heptane mechanisms with a size <70 species are tested in the present study. The ignition characteristics of methane and *n*-heptane for these mechanisms are first evaluated by performing zero-dimensional (0-D) homogeneous reactor (HR) calculations for a pressure range of 36–48 atm and equivalence ratio of 0.4. Results from all three mechanisms show good agreement with measurements. Next, computational fluid dynamic simulations of a *n*-heptane spray in a premixed methane/air mixture are carried out using the three mechanisms, in which the ambient temperature and density are set to 900 K and 14.8 kg/m³, respectively. Dual-fuel is considered by varying the equivalence ratio of methane (ϕ_{CH_4}) in the ambient gas from 0 to 0.5. The ignition delay time of the pure *n*-heptane spray is predicted to be within 21% as compared to measured data. It is shown that despite having reasonable performance in 0-D HR calculations, the ignition process in dual-fuel spray combustion varies for different mechanisms which may affect the conclusion of a study. Therefore, an extensive model evaluation is required prior to actual application.

Keywords: diesel spray flame, dual-fuel, ignition delay, chemical mechanism, computational fluid dynamics

1. INTRODUCTION

The use of natural gas as a main fuel to power internal combustion engines for maritime transportation

is of international interest to fulfill the ever more stringent emission standards. A significant reduction of NO_x and soot emissions can be achieved due to the low carbon-to-hydrogen ratio of natural gas. However, the low reactivity of lean premixed charges renders reliable ignition difficult. Therefore, a micro-pilot injection of a highly reactive liquid fuel is used to ensure successful combustion initiation in dual-fuel engines. Methane is generally treated as the representative of natural gas due to the high methane content of natural gas. The cetane number of *n*-heptane is close to that of diesel, and thus *n*-heptane is taken as the single-component surrogate fuel of diesel. It has been observed in engine experiments that the ignition of diesel spray is retarded if the ambient air contains methane [1, 2]. This is confirmed by numerous experimental studies which were carried out in fundamental reactors, such as shock tube (ST) [3, 4], rapid compression machine [2].

To gain a better understanding of the ignition process, numerical simulations are carried out. Zero-dimensional (0-D) homogeneous reactor (HR) calculations were performed to have more insights on the role of each reactions during methane/*n*-heptane ignition [3, 4, 5, 6]. In all cases, methane addition is shown to delay the ignition of *n*-heptane mixture. In a constant volume chamber, Wei et al. [6] and Zhao et al. [7] performed large eddy simulation of *n*-heptane spray in methane environment using a reduced *n*-heptane mechanism [8]. It was similarly shown that increasing methane concentration in the ambient mixture increases the ignition delay time (IDT) of the *n*-heptane spray. However, it is important to note that only a single chemical mechanism, which includes methane subset,

was employed in their study of dual-fuel combustion. The choice of mechanism was based on 0-D HR calculations. It is shown in [9] that different mechanisms, despite having similar performance during 0-D HR calculations, have different low temperature chemistry which strongly impact the evolution of the flame structure. Setting against this background, the present study aims to evaluate the performance of different reduced *n*-heptane mechanisms in dual-fuel combustion. This is achieved by performing both 0-D HR calculations and three-dimensional (3-D) computational fluid dynamic (CFD) spray modeling.

2. CHEMICAL KINETIC MODELS

Three reduced *n*-heptane mechanisms are considered in the present study to evaluate their *n*-heptane and methane combustion characteristics. The names of the mechanisms, the number of species, and the number of reactions are provided in Table 1. Detailed description of each mechanism can be referred to in their respective publication. To evaluate the *n*-heptane and methane combustion characteristics, the present work employs a 0-D HR model from the ANSYS CHEMKIN for IDT calculations. The reactor model is assumed to be a closed, homogeneous, constant volume and adiabatic system. The IDT is defined as the time where the maximum rate of temperature rise in the system. In addition, laminar flame speed (LFS) is also computed to complement the IDT results. However, only the LFS calculation for methane is carried out.

Table 1: The chemical mechanisms utilized in the present study.

Name	No. of Species	No. of Reactions	Ref.
Liu44	44	112	[8]
Seidel56	56	128	[10]
Lu68	68	283	[11]

3. CFD SETUP

The operating conditions as well as the nozzle diameter (D_{noz}) specification for each test cases are listed in Table 2. These cases correspond to the grade number two Diesel fuel (Diesel #2) spray experimental data [12, 13]. The injection pressure for all the cases are set to 1400 bar. The injected fuel mass flow rate for the D_{noz} cases of 257 and 180 μm are set to 14.0 and 8.8 mg/ms, respectively. Cases 1 – 3 are non-reacting spray cases, where the ambient oxygen concentration (O_2) is set to zero. Cases 4 – 7 are reacting spray cases where O_2 and ambient temperature (T_{am}) are set to 21% by mole fraction and 900 K, respectively. Meanwhile, the methane concentration, which is represented by the

equivalence ratio of methane (ϕ_{CH_4}), varies across different cases. The ambient mixture composition is shown in Table 3.

The test cases listed in Table 2 are simulated by performing 3-D CFD spray combustion simulations using OpenFOAM-v1712. The computational domain is a constant volume cubic chamber with side lengths of 108 mm, which corresponds to the volume of the experimental combustion vessel [12]. The injector is placed at the center of one of the chamber walls. The mesh configuration used in [14] is employed in the present study which involves an isotropic cell size of 0.5 mm within the spray combustion region. This mesh configuration was shown to reach mesh independence in [14]. The time step size is fixed at 0.2 μs .

Table 2: Operating conditions and nozzle specification.

Case	D_{noz} [μm]	T_{am} [K]	ρ_{am} [kg/m^3]	O_2 [% mole]	ϕ_{CH_4} [-]
1	257	900	13.9	0.00	0.0
2	257	1000	13.9	0.00	0.0
3	180	900	14.8	0.00	0.0
4	180	900	14.8	21.00	0.0
5	180	900	14.8	21.00	0.3
6	180	900	14.8	21.00	0.4
7	180	900	14.8	21.00	0.5

Table 3: Ambient gas composition.

ϕ_{CH_4}	0.0	0.0	0.3	0.4	0.5
O_2	0.00	21.00	21.00	21.00	21.00
CO_2	6.52	6.11	5.87	5.79	5.70
H_2O	3.77	3.56	3.42	3.37	3.32
N_2	89.71	69.33	66.56	65.64	64.73
CH_4	0.00	0.00	3.15	4.20	5.25

The fuel spray, flow and combustion processes are modeled using the Eulerian-Lagrangian approach within the unsteady Reynolds averaged Navier-Stokes framework. The realizable *k*-epsilon model is employed for turbulence modeling. Primary breakup is considered by injecting computational parcels with the Rosin-Rammler distribution. The secondary breakup is modeled by the Reitz-Diwakar spray model, in which the stripping break up constant, C_s is set to 6. The well-stirred reactor (WSR) combustion model is employed in the present study. It is coupled with the Chemistry Coordinate Mapping (CCM) approach to speed up the integration process of the chemical reaction rates [15]. The current work uses the same CCM settings as in [15].

4. RESULTS AND DISCUSSION

4.1 Performance of chemical mechanisms

4.1.1 Ignition delay time for *n*-heptane

Figure 1 compares the IDT of *n*-heptane/air mixture from different mechanisms against measurement data [16] at ambient pressure (P_{am}) of 42 atm, and the equivalence ratio of *n*-heptane ($\phi_{C_7H_{16}}$) of 1.0, respectively. As illustrated in Figure 1, both Liu44 and Seidel56 show good agreement with the experimental data. However, an overprediction is observed for Lu68 at temperature of 1000 K. This is likely due to the inherent characteristic from the detailed *n*-heptane mechanism [17] it is derived from, as the detailed mechanism also showed similar discrepancy (not shown). Despite this, the NTC region is well captured by all three mechanisms.

4.1.2 Ignition delay time and laminar flame speed for methane

In this section, the methane characteristics of different mechanisms are evaluated. Figure 2 illustrates the IDT of methane/oxygen mixture at fuel-lean mixture of $\phi_{CH_4} = 0.4$ and $P_{am} = 48$ atm. From Figure 2a, all the tested mechanisms agree with the measurements [18] under fuel-lean condition. The methane characteristics of different mechanisms are also evaluated by their performance in predicting LFS. Comparison of the predicted LFS from different mechanisms at P_{am} of 1 and 10 atm, as well as the measurement data from [19] are illustrated in Figure 3. As shown in the figure, the LFS predictions by Lu68 and Liu44 are overpredicted at P_{am} of 1 atm, with a maximum relative error of 40% and 19%,

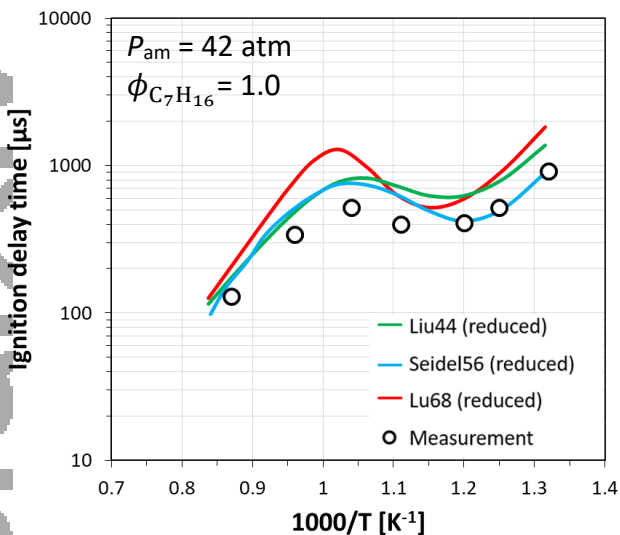


Figure 1: Comparison of ignition delay times of *n*-heptane/air mixture at $P_{am} = 42$ atm and $\phi_{C_7H_{16}} = 1.0$ for different mechanisms and measurement data [16].

respectively, to measured data. Meanwhile, Seidel56 corresponds better with the measurement data where the relative errors are within 15% for $\phi_{CH_4} \leq 1.2$. However, an error of 32% is observed at $\phi_{CH_4} = 1.3$. As P_{am} increases to 10 atm, both Liu44 and Seidel56 now underpredict the LFS by a maximum relative difference of 45%. Conversely, the predicted LFS by Lu68 now has a much better agreement with measurement data by having relative errors < 22%. Overall, the three reduced mechanisms are able to capture the measurement trend where LFS decreases as P_{am} increases. Overall, all three reduced mechanisms show reasonable performance in capturing the *n*-heptane and methane characteristics. Therefore, the three reduced mechanisms are tested next in 3-D dual-fuel spray combustion simulations.

4.2 Validation of spray combustion setup

4.2.1 Non-reacting spray

Before performing reacting spray simulations, the computational setup is first validated by comparing the liquid penetration length (LPL) and vapor penetration length (VPL) from non-reacting spray simulations against measurement data [20]. The experimental VPL data for D_{noz} of 180 μm is not available. Hence, the VPL measurement for the D_{noz} of 257 μm is used to evaluate the model. For the LPL, the comparison is made against the LPL determined with the liquid length scaling law [13]. The liquid properties of *n*-heptadecane are used in the liquid scaling law to produce Diesel #2 liquid length [13] since these resemble the properties of Diesel #2. In the present study, LPL is defined as axial maximum distance between the spray injector nozzle and the

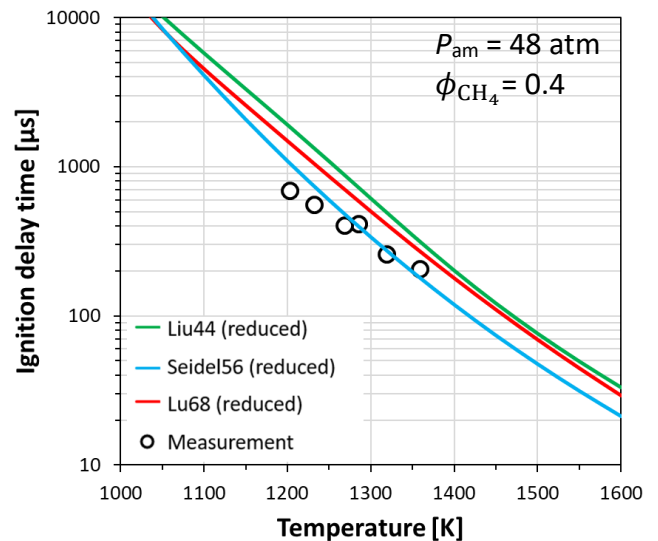


Figure 2: Comparison of ignition delay times of fuel-lean (3.8% $CH_4 + 19.2\%$ O_2 in Ar, $\phi_{CH_4} = 0.4$, $P_{am} = 48$ atm) mixtures for different mechanisms and measurement data [18].

position where 95 % of the total liquid mass is observed; VPL is determined using the farthest downstream location of 0.1 % fuel mass fraction. Comparison of LPL and VPL for D_{noz} of 180 and 257 μm are shown in Figure 4. As illustrated in the figure, the numerical setup is able to replicate the experimental LPL and VPL reasonably well. Therefore, the same setup is next used in simulating the reacting spray cases.

4.2.2 Reacting spray

Validation of the combustion characteristics is carried out by comparing the IDT of the reacting diesel spray case (Case 4) with measurement data. The simulated IDTs from three different reduced n -heptane mechanisms are presented in Figure 5a. The computed IDTs have the same definition as the measurement data [12], which is the time from start of injection to the time when the maximum rate of maximum temperature rise in the domain occurs. As illustrated in Figure 5a, the predicted IDTs by Seidel56 and Lu68 correspond with the experimental data by having a maximum difference of 3.3%. However, Liu44 is shown to overpredict the IDT by approximately 21% relative to the measured data.

4.3 Effect of ϕ_{CH_4} on ignition delay time

The predicted IDTs from different reduced n -heptane mechanisms as methane concentration increases are illustrated in Figure 5a. From the figure, all three reduced mechanisms show increasing IDT as methane concentration increases, which agrees with the literature work [2]. However, the magnitude of the IDT change relative to the pure diesel case varies differently across the three mechanisms as methane concentration

increases. Liu44 is shown to be the least sensitive to methane addition as the predicted IDT at $\phi_{CH_4} = 0.5$ is only 2.3% longer than in the pure n -heptane case ($\phi_{CH_4} = 0.0$). On the other hand, both Seidel56 and Lu68 show significant increase in IDT by 46% and 33%, respectively.

Further analysis is carried out by plotting the temporal evolution of maximum temperature (T_{max}) in the system, which is illustrated in Figure 5b and 5c. By examining the T_{max} profile for Liu44 (Figure 5b), a noticeable delay in the rise of T_{max} is observed when $\phi_{CH_4} = 0.3$. However, the subsequent addition of methane up to $\phi_{CH_4} = 0.5$ only shows minor effect on the T_{max} profile. This agrees with the IDT trend seen in Figure 5a. On the other hand, methane addition shows significant effect on the T_{max} profile in the Seidel56 and Lu68 cases. In Seidel56 (Figure 5c), a slight delay of approximately 0.05ms is observed in the onset of temperature rise when $\phi_{CH_4} = 0.3$. However, a further increase of ϕ_{CH_4} to 0.5 has minor effects on the onset time. It is notable from Figure 5c that the T_{max} profiles for all ϕ_{CH_4} values converges at a temperature slightly above 1000 K. From this convergence point onwards, significant delay in the time of temperature rise is observed as methane concentration level increases. This leads to the longer IDT observed in Figure 5a. This observation is, however, not captured in the Lu68 case. Instead, the methane addition is shown in Figure 5d to significantly delay the onset of temperature rise.

Based on the results shown in Figure 5, it is suspected that methane addition affects the low- and high-temperature ignition stages differently for different mechanisms. In Liu44, methane addition shows insignificant effect on the onset timing of temperature

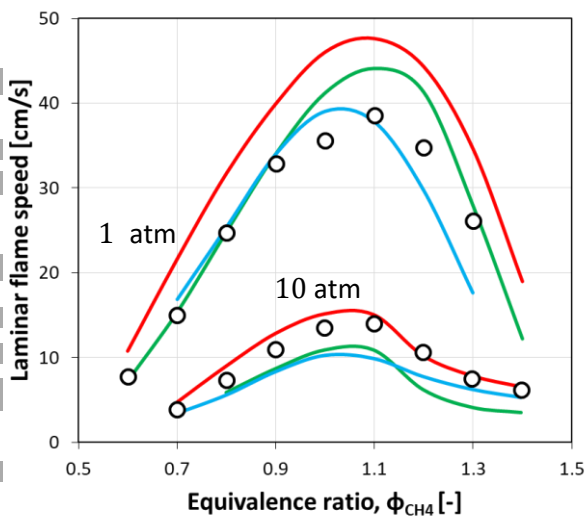


Figure 3: Predicted laminar flame speed of methane/air mixture at P_{am} of 1 atm and 10 atm with an initial temperature of 300 K for different mechanisms and compared against measurement data [19]. Please refer to Figure 2 for the legends.

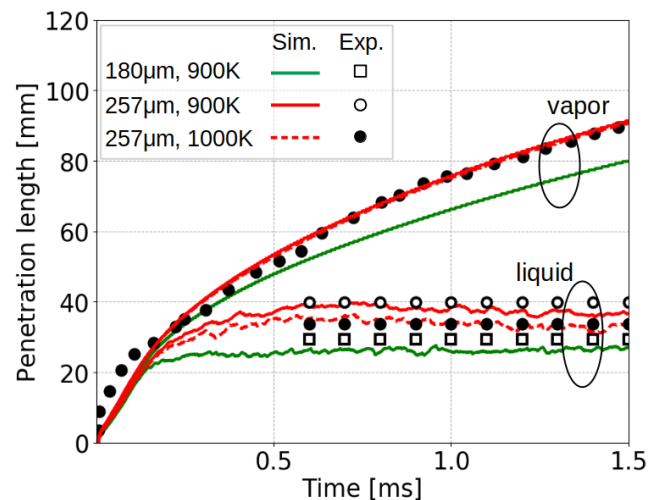


Figure 4: Comparison of experimental and simulated penetration lengths. Note that the experimental LPL is produced using the liquid length scaling law [13].

rise. Only until the temperature has risen to >950K that an observable effect can be seen. In Seidel56, methane addition is also shown to have minor effect on the onset timing of temperature rise, while a significant effect is only observed at $T > 1000\text{K}$. This implies that the high temperature reactions in both Liu44 and Seidel56 are more susceptible to the presence of methane. In contrast, methane addition is shown to delay the onset of temperature rise in Lu68 cases, but have a minor effect during high temperature rise. This result suggests that the low-temperature reaction in Lu68 is more sensitive to the presence of methane. Furthermore, it is noteworthy that the transition from low-temperature ignition to high-temperature ignition are obviously seen in both Seidel56 and Lu68 cases (cf. Figures 5c and 5d), but not in Liu44. This may be the reason for Liu44 being less sensitive to methane addition as shown in Figure 5a.

5. CONCLUSION

Numerical simulations are carried out to evaluate the performance of different reduced *n*-heptane mechanisms in dual-fuel ignition. Three mechanisms (Liu44, Seidel56, and Lu68) are evaluated using 0-D homogeneous reactor (HR) models. This is followed by performing 3-D CFD simulations of *n*-heptane spray into premixed methane/air mixture. The 0-D HR model calculation is carried out at pressures and equivalence ratios of 36 – 48 atm and 0.4, respectively. The CFD simulations are carried out at an ambient temperature and density of 900 K and 14.8 kg/m³, respectively. Dual-fuel is considered by varying the equivalence ratio of methane (ϕ_{CH_4}) in the ambient gas from 0 to 0.5.

The three mechanisms are shown to have reasonable prediction of methane and *n*-heptane ignition delay time (IDT) in the 0-D HR model. On the other hand, the predicted *n*-heptane IDTs in CFD simulations are within a maximum relative difference of 21% to measured data. As methane concentration increases to $\phi_{\text{CH}_4} = 0.5$, IDTs for all three mechanisms are delayed but with different magnitude. The IDT for Liu44 is shown to increase by 2.3%, while the IDTs for Seidel56 and Lu68 increase significantly by 46% and 33%, respectively. An examination of the maximum temperature profiles for different reduced mechanisms shows that methane addition have different effect on each mechanism. Methane is shown to have a relatively dominant effect on the high-temperature ignition stage in the Liu44 and Seidel56 cases. In contrast, the low-temperature ignition stage is more significantly affected by methane in the Lu68 case. The results suggest that

different mechanisms behaves differently during dual-fuel combustion which may lead to different conclusions. Therefore, the choice mechanism is critical.

ACKNOWLEDGEMENT

The authors gratefully acknowledge the financial support from the Independent Research Fund Denmark (DFF) and MAN Energy Solutions under the grant number 8022-00143B. The computations were performed using the Niflheim cluster at Technical University of Denmark.

REFERENCE

- [1] Lee CS, Lee KH, Kim DS. Experimental and numerical study on the combustion characteristics of partially premixed charge compression ignition engine with dual fuel. *Fuel*. 2003;82(5):553-60.
- [2] Schlatter S, Schneider B, Wright YM, Boulouchos K. *n*-heptane micro pilot assisted methane combustion in a Rapid Compression Expansion Machine. *Fuel*. 2016;179:339-52.
- [3] Liang J, Zhang Z, Li G, Wan Q, Xu L, Fan S. Experimental and kinetic studies of ignition processes of the methane–*n*-heptane mixtures. *Fuel*. 2019;235:522-9.
- [4] Gong Z, Feng L, Wei L, Qu W, Li L. Shock tube and kinetic study on ignition characteristics of lean methane/*n*-heptane mixtures at low and elevated pressures. *Energy*. 2020:117242.
- [5] Aggarwal SK, Awomolo O, Akber K. Ignition characteristics of heptane–hydrogen and heptane–methane fuel blends at elevated pressures. *Int J Hydrogen Energ*. 2011;36(23):15392-402.
- [6] Wei H, Qi J, Zhou L, Zhao W, Shu G. Ignition characteristics of methane/*n*-heptane fuel blends under engine-like conditions. *Energ Fuel*. 2018;32(5):6264-77.
- [7] Zhao W, Zhou L, Liu Z, Qi J, Lu Z, Wei H, Shu G. Numerical Study on the Combustion Process of *n*-heptane Spray Flame in Methane Environment Using Large Eddy Simulation. *Combust Sci Technol*. 2019:1-25.
- [8] Liu S, Hewson JC, Chen JH, Pitsch H. Effects of strain rate on high-pressure nonpremixed *n*-heptane autoignition in counterflow. *Combust Flame*. 2004;137(3):320-39.
- [9] Payri F, García-Oliver JM, Novella R, Pérez-Sánchez EJ. Influence of the *n*-dodecane chemical mechanism on the CFD modelling of the diesel-like ECN Spray A flame structure at different ambient conditions. *Combust Flame*. 2019;208:198-218.
- [10] Seidel L, Netzer C, Hilbig M, Mauss F, Klauer C, Pasternak M, Matrisciano A. Systematic reduction of detailed chemical reaction mechanisms for engine applications. *J Eng Gas Turbine Power*. 2017;139(9).

[11] Lu T, Law CK, Yoo CS, Chen JH. Dynamic stiffness removal for direct numerical simulations. *Combust Flame*. 2009;156(8):1542-51.

[12] Engine Combustion Network. <https://ecn.sandia.gov>. 2020;

[13] Siebers DL. Scaling liquid-phase fuel penetration in diesel sprays based on mixing-limited vaporization. *SAE Trans*. 1999:703-28.

[14] Pang KM, Jangi M, Bai XS, Schramm J, Walther JH, Glarborg P. Effects of ambient pressure on ignition and flame characteristics in diesel spray combustion. *Fuel*. 2019;237:676-85.

[15] Jangi M, Bai XS. Multidimensional chemistry coordinate mapping approach for combustion modelling with finite-rate chemistry. *Combust Theor Model*, 2012; 16: 1109-32

[16] Ciezki HK, Adomeit G. Shock-tube investigation of self-ignition of *n*-heptane-air mixtures under engine relevant conditions. *Combust Flame*. 1993;93(4):421-33.

[17] Curran HJ, Gaffuri P, Pitz WJ, Westbrook CK. A comprehensive modeling study of *n*-heptane oxidation. *Combust Flame*. 1998;114(1-2):149-77.

[18] Davidson DF, Hanson RK. Fundamental kinetics database utilizing shock tube measurements. Mechanical Engineering Department, Stanford University, Stanford CA. 2005 Jul 25.

[19] Rozenchan G, Zhu DL, Law CK, Tse SD. Outward propagation, burning velocities, and chemical effects of methane flames up to 60 atm. *Proc Combust Inst*. 2002;29(2):1461-70.

[20] Naber JD, Siebers DL. Effects of gas density and vaporization on penetration and dispersion of diesel sprays. *SAE Trans*. 1996:82-111.

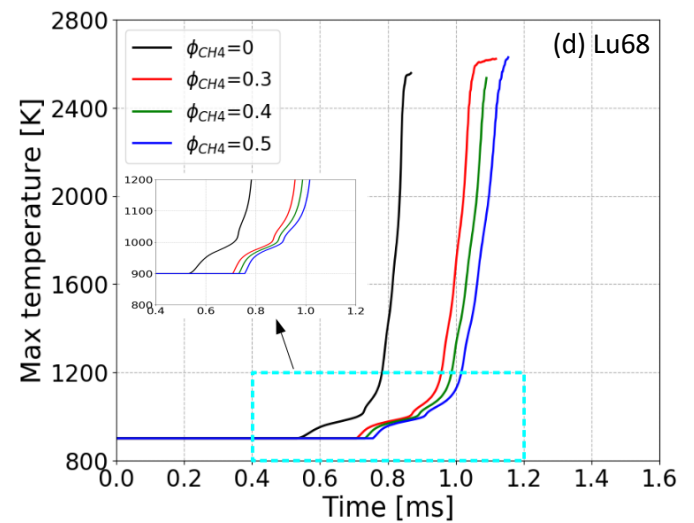
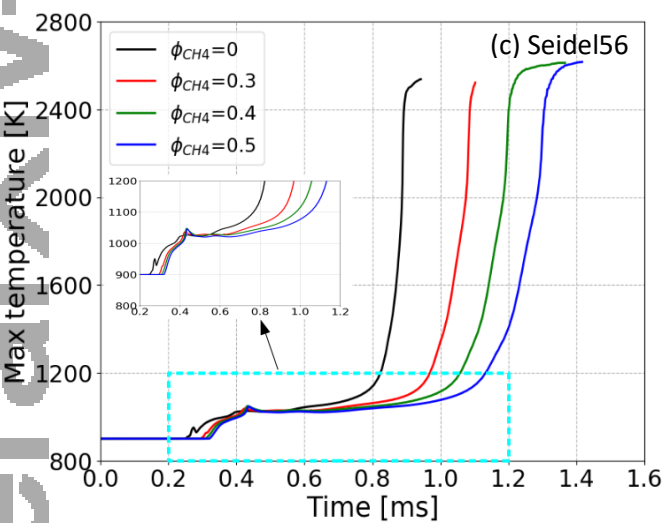
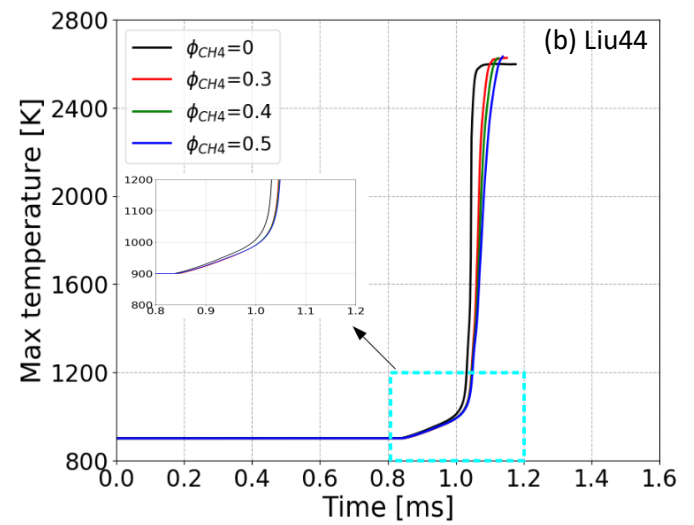
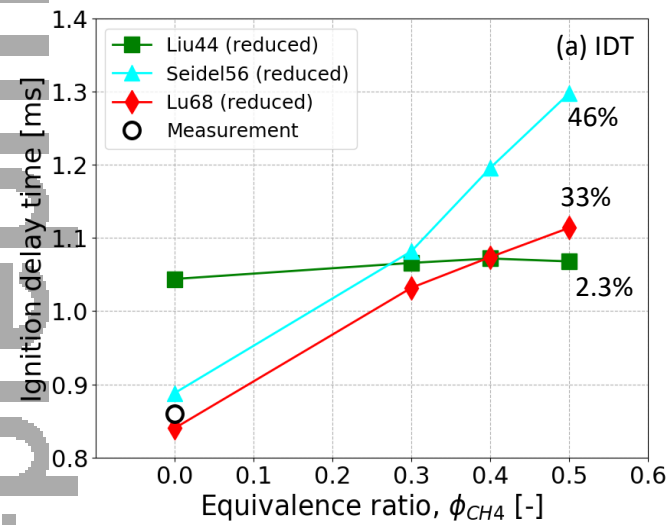


Figure 5: (a) Ignition delay time (IDT) for different mechanisms at varying ϕ_{CH_4} values for D_{noz} of 180 μ m and T_{am} of 900 K. The temporal evolution of maximum temperature for (b) Liu44, (c) Seidel56, and (d) Lu68 with varying ϕ_{CH_4} values.